JOURNAL OF GUIDANCE, CONTROL, AND DYNAMICS
Vol. 32, No. 2, March–April 2009

Gust Energy Extraction for Mini and Micro Uninhabited Aerial Vehicles

Jack W. Langelaan*
Pennsylvania State University, University Park, Pennsylvania 16802

DOI: 10.2514/1.37735

This paper discusses energy extraction from atmospheric turbulence by small and micro uninhabited aerial vehicles. A nonlinear longitudinal dynamic model of a glider with elevators as the sole control input is used for the aircraft, and feedback control laws for energy extraction are discussed. An expression for energy change with respect to distance for flight in a spatially varying wind field is derived, and this is used with measurements of wind speed and gradient to compute the state that maximizes the instantaneous gain in total energy. A state feedback controller uses elevator input to regulate states to the optimal values. The state feedback control law is computed using linear quadratic regulator synthesis, and the state and input weight matrices that maximize energy gain are found using a search method. Simulation results of flights through sinusoidal gust fields and random thermal fields show the performance of the proposed approach.

I. Introduction

A MAJOR handicap associated with small and micro unmanned aerial vehicles (SMUAVS) is the limited onboard energy capacity (either as chemical fuel or as batteries). The reduced endurance and range that result greatly reduce the utility of such vehicles. Additionally, the low Reynolds numbers inherent to SMUAVS make it very difficult to achieve lift/drag ratios that are comparable with larger aircraft, further reducing overall performance.

However, significant energy is available from the atmosphere. Large birds and human sailplane pilots routinely exploit vertical air motion (lift) to remain aloft for several hours and fly hundreds of kilometers without flapping wings or the use of engines. Exploiting these long-duration vertical air motions has been an active area of research for manned glider flight for many years and is now becoming of interest for small unmanned aerial vehicles (UAVs) as well.

In addition to the relatively long-duration air motion exploited by sailplane pilots, energy is also available from short-duration phenomena such as gusts. It has been observed by radio-control glider pilots that flight performance relative to birds is significantly reduced on a gusty day [1]. This implies that birds are exploiting gusts to minimize the effect on performance (and may in fact be able to improve performance), a feat that human radio-control pilots are not able to reproduce. Kiceniuk [2] reports that it is even possible to extract energy from a downward gust. Extracting energy from gusts is complicated by their typically short duration, and hence very fast response (usually exceeding human reaction time) is required. Although traditional flight control methods have focused on mitigating the effects of disturbances such as gusts, the research proposed here seeks to exploit disturbances to enhance range and endurance.

Urban environments are particularly gusty and thus will greatly affect the flight performance of a small or micro air vehicle. Hence, exploiting atmospheric disturbances such as gusts has the potential to significantly increase the utility of small flight vehicles operating in urban environments. Although a significant amount of work has been done on exploiting longer-duration atmospheric effects (for example, the autonomous soaring research described by Allen and Lin [3]) and dynamic soaring (i.e., exploiting spatial gradients in a wind field [1]), less work has been performed on exploiting gusts. Phillips [4] describes an approach to compute an equivalent thrust coefficient that occurs due to vertical gusts and concluded that the effect is too small to be useful in crewed aircraft. A major factor determining the energy that can be extracted from gusts is the ratio of gust velocity to air speed, and this is generally too small in full-sized aircraft. However, extending Phillips's approach to small and micro UAVS (with their correspondingly lower air speeds) shows that significant performance improvement is possible for this scale of flight vehicle.[†]

Earlier approaches that generated control laws based on lift coefficient [5] and load factor [6] showed potential for energy savings of up to 40% when gust-soaring techniques were employed.

This paper presents a closed-loop architecture for gust energy extraction using a full model for aircraft longitudinal dynamics. Although the methodology for control law development is general to powered SMUAVS and aircraft equipped with flaps, we present results for a small autonomous glider with only elevator inputs. The focus here is extended range and endurance for cruising flight; other problems associated with flight in urban environments (for example, obstacle avoidance) are not addressed.

The remainder of this paper is organized as follows: Section II provides a brief review of previous work, Sec. III discusses the dynamics and energetics of vehicle flight in gusts, Sec. IV describes the control architecture and control law development, Sec. V presents simulation results of flights through sinusoidal gust fields and flight through a thermal field, and Sec. VI concludes the work.

II. Previous and Related Research

Driven by competition glider flying, a significant amount of work has been reported on optimal piloting techniques for static soaring. One of the most famous (and certainly most widely adopted) techniques was published by MacCready [7], which describes what is now known as MacCready speed to fly theory. Other selected examples include Arho [8], who examine minimum time soaring with a minimum altitude constraint; Metzger and Hedrick [9], who describe maximum speed with no net altitude loss; de Jong [10], who discuss a geometric approach to sailplane trajectory optimization;

Presented as Paper 223 at the 46th AIAA Aerospace Sciences Meeting and Exhibit, Reno, NV, 7–10 January 2008; received 26 March 2008; revision received 28 August 2008; accepted for publication 28 August 2008.

*Assistant Professor, Department of Aerospace Engineering. Senior Member AIAA.

[†]Note that if one can find a region of the atmosphere in which gust velocities begin to approach the order of magnitude of air speed of a full-sized aircraft, then one may be able perform useful energy extraction even with crewed aircraft. However, this is likely to result in an extremely uncomfortable ride.

and, somewhat more recently, Cochrane [11], who extend MacCready theory to uncertain lift.

The trajectory optimization literature generally uses a simplified glider model, which assumes that the pilot has direct control of air speed. This assumption is certainly appropriate for long-duration flights in which the glider spends most of its time in a trimmed condition, but this assumption is not valid for periods of transition between trimmed conditions. Some authors have addressed optimal transitions to minimize energy loss [12,13], and Gedeon [14] describes an analysis of dolphin-style flight through thermals.

Dynamic soaring by both aircraft and birds has again become an active area of research. Optimal trajectories for energy extraction from wind gradients are described by Zhao [15], and minimum fuel trajectories for power-assisted dynamic soaring are described by Zhao and Qi [16]. Dynamic soaring using shear layers is described by Sachs and Mayrhofer [17], and elsewhere they discuss the minimum wind shear strength required for albatross flight [18]. Pennycuick [19] proposes an alternate flight mode in which most of the energy gain is obtained from the shear layer that results from the wind's flow separation over the crest of each wave. Successful exploitation of this strategy requires sensing very small changes in dynamic pressure, and he suggested that only tube-nosed birds such as albatrosses have the necessary sensory capability.

Energy extractions from both thermals and dynamic soaring are generally considered to be deterministic problems. Gusts are inherently stochastic, are much shorter in duration, and generally show far greater spatial variation. This makes effective energy extraction more difficult. In addition, because useful energy extraction from gusts is only practical for small UAVS, it has received comparatively less attention. Previously mentioned work by Lissaman [20], Patel and Kroo [5], and Lissaman and Patel [6] uses a point mass model for the aircraft, thus ignoring potentially important dynamics.

III. Vehicle Dynamics and Energetics

For simplicity, only longitudinal motion is considered. Following a derivation similar to that presented by Pierson and Chen [21], consider an aircraft located at $\mathbf{r}$ in an inertial frame I, where $\hat{x}^i$ and $\hat{z}^i$ define unit vectors (see Fig. 1).

Using a common definition of stability axes, define $\hat{x}^s$ as a unit vector in the direction of air speed (so that $\mathbf{v} = v_a\hat{x}^s$) and $\hat{z}^s$ opposite to lift. The velocity of the aircraft in the inertial frame is the sum of the velocity of the aircraft in the stability axes and the wind velocity:

$$\dot{\mathbf{r}} = \mathbf{v} + \mathbf{w} \tag{1}$$

Hence,

$$\ddot{\mathbf{r}} = \frac{\mathrm{d}}{\mathrm{d}t}\mathbf{v} + \frac{\mathrm{d}}{\mathrm{d}t}\mathbf{w} \tag{2}$$

The angle γ defines the rotation between the stability axes and the inertial axes, and it is the flight-path angle with respect to the surrounding air mass. When $\mathbf{w} = 0$, it is also the flight-path angle with respect to the inertial frame. In this application, γ is defined as positive upward, and so for a steady glide, the glideslope with respect to the air mass is negative. The acceleration of the aircraft is

$$\frac{\mathrm{d}}{\mathrm{d}t}\mathbf{v} = \dot{v}_a\hat{x}^s + \boldsymbol{\omega}^s \times v_a\hat{x}^s \tag{3}$$

Substituting $\boldsymbol{\omega}^s = \dot{\gamma}\hat{y}^s$ gives

$$\frac{\mathrm{d}}{\mathrm{d}t}\mathbf{v} = \dot{v}_a\hat{x}^s - \dot{\gamma}v_a\hat{z}^s \tag{4}$$

Therefore,

$$\mathbf{L} + \mathbf{D} + m\mathbf{g} + \mathbf{T} = m\left[\dot{v}_a\hat{x}^s - \dot{\gamma}v_a\hat{z}^s + \frac{\mathrm{d}}{\mathrm{d}t}\mathbf{w}\right] \tag{5}$$

where $\mathbf{L}$ is the lift vector, $\mathbf{D}$ is the drag vector, $\mathbf{g}$ is the acceleration due to gravity, $\mathbf{T}$ is the thrust vector, and m is the mass. Lift and drag are generally expressed in the stability frame, thrust is generally expressed in the body frame, and gravity is generally expressed in the inertial frame:

$$\mathbf{L} = -\tfrac{1}{2}\rho v_a^2 S C_L \hat{z}^s \tag{6}$$

$$\mathbf{D} = -\tfrac{1}{2}\rho v_a^2 S C_D \hat{x}^s \tag{7}$$

$$\mathbf{T} = \tfrac{1}{2}\rho v_a^2 S C_T \hat{x}^b \tag{8}$$

$$\mathbf{g} = g\hat{z}^i \tag{9}$$

The kinematics of the aircraft can now be defined in terms of the air speed, flight-path angle, and wind speed. It is generally more convenient to work in terms of pitch angle and angle of attack, and Fig. 1 shows that $\gamma = \theta - \alpha$:

$$\dot{x}_i = v_a\cos(\theta - \alpha) + w_x \tag{10}$$

$$\dot{z}_i = -v_a\sin(\theta - \alpha) + w_z \tag{11}$$

$$\dot{\theta} = Q \tag{12}$$

where Q is the pitch rate.

Substituting Eqs. (6–9) into Eq. (5) and writing in component form, vehicle dynamics are expressed in stability axes as

$$\dot{v}_a = q\frac{S}{m}(C_T\cos\alpha - C_D) - \frac{\mathrm{d}w_x}{\mathrm{d}t}\cos(\theta - \alpha) + \left(\frac{\mathrm{d}w_z}{\mathrm{d}t} - g\right)\sin(\theta - \alpha) \tag{13}$$

$$\dot{\alpha} = Q - q\frac{S}{v_a m}(C_L + C_T\sin\alpha) - \frac{1}{v_a}\frac{\mathrm{d}w_x}{\mathrm{d}t}\sin(\theta - \alpha) - \frac{1}{v_a}\left(\frac{\mathrm{d}w_z}{\mathrm{d}t} - g\right)\cos(\theta - \alpha) \tag{14}$$

$$\dot{Q} = q\frac{ScC_m}{I_{yy}} \tag{15}$$

where $q = \frac{1}{2}\rho v_a^2$.

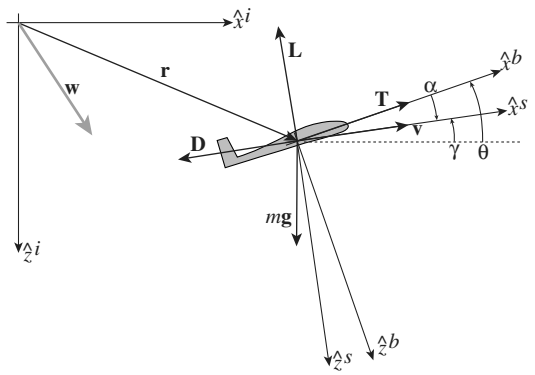

Fig. 1 Reference frames in which positive rotations are indicated, and so positive glideslope is upward and angle of attack is positive in the conventional sense.

The aerodynamic coefficients are adapted from those presented elsewhere [22]:

$$C_L = C_{L0} + C_{L_\alpha}\alpha + \frac{c}{2v_a}(C_{L_Q}Q + C_{L_{\dot\alpha}}\dot\alpha) + C_{L_{\delta_e}}\delta_e + C_{L_{\delta_f}}\delta_f \tag{16}$$

$$C_D = f_{LD}(C_{L0} + C_{L_\alpha}\alpha) + C_{D_{\delta_e}}\delta_e + C_{D_{\delta_f}}\delta_f \tag{17}$$

$$C_m = C_{m0} + C_{m_\alpha}\alpha + \frac{c}{2v_a}C_{m_Q}Q + C_{m_{\delta_e}}\delta_e + C_{m_{\delta_f}}\delta_f \tag{18}$$

where $f_{LD}(C_{L0} + C_{L_\alpha}\alpha)$ is a polynomial function that relates drag coefficient to lift coefficient. Control inputs are thrust coefficient C_T, elevator deflection δ_e, and flap deflection δ_f. Here, it is assumed that actuator response is very fast compared with vehicle dynamics, and thus actuator dynamics are neglected.

A. Total Energy

The vehicle's specific total energy (i.e., total energy divided by mass) is

$$E_{\text{tot}} = gh + \tfrac{1}{2}(\dot x_i^2 + \dot z_i^2) \tag{19}$$

where h is the height above a datum. Substituting vehicle kinematics,

$$E_{\text{tot}} = gh + \tfrac{1}{2}(v_a^2 + 2v_a w_x \cos\gamma - 2v_a w_z \sin\gamma + w_x^2 + w_z^2) \tag{20}$$

The rate of change of specific energy is

$$\begin{aligned}\dot E_{\text{tot}} = {} & g\dot h + v_a\dot v_a + \dot v_a w_x\cos\gamma + v_a\dot w_x\cos\gamma - \dot\gamma v_a w_x\sin\gamma \\ & - \dot v_a w_z\sin\gamma - v_a\dot w_z\sin\gamma - \dot\gamma v_a w_z\cos\gamma + \dot w_x w_x + \dot w_z w_z\end{aligned} \tag{21}$$

Gathering terms and letting $\dot h = v_a\sin\gamma - w_z$,

$$\begin{aligned}\dot E_{\text{tot}} = {} & g(v_a\sin\gamma - w_z) + \dot v_a(v_a + w_x\cos\gamma - w_z\sin\gamma) \\ & - \dot\gamma(v_a w_x\sin\gamma + v_a w_z\cos\gamma) + \dot w_x(v_a\cos\gamma + w_x) \\ & + \dot w_z(-v_a\sin\gamma + w_z)\end{aligned} \tag{22}$$

Substituting vehicle dynamics and setting $\theta - \alpha = \gamma$,

$$\begin{aligned}\dot E_{\text{tot}} = {} & q\frac{S}{m}[(v_a\cos\alpha + w_x\cos\theta - w_z\sin\theta)C_T \\ & - (w_x\sin\gamma + w_z\cos\gamma)C_L - (v_a + w_x\cos\gamma - w_z\sin\gamma)C_D] \\ & - v_a(\dot w_x\cos\gamma - \dot w_z\sin\gamma) - w_x\dot w_x - w_z\dot w_z\end{aligned} \tag{23}$$

Here, we assume that the wind field is frozen in space; thus,

$$\frac{\mathrm{d}}{\mathrm{d}t}\mathbf{w} = \nabla\mathbf{w}\begin{bmatrix}\dot x_i \\ \dot z_i\end{bmatrix} = \begin{bmatrix}\frac{\delta w_x}{\delta x_i}\dot x_i + \frac{\delta w_x}{\delta z_i}\dot z_i \\ \frac{\delta w_z}{\delta x_i}\dot x_i + \frac{\delta w_z}{\delta z_i}\dot z_i\end{bmatrix} \tag{24}$$

where $\nabla\mathbf{w}$ is the spatial gradient of the wind vector. The rate of change of total energy is therefore

$$\begin{aligned}\dot E_{\text{tot}} = {} & q\frac{S}{m}[(v_a\cos\alpha + w_x\cos\theta - w_z\sin\theta)C_T \\ & - (w_x\sin\gamma + w_z\cos\gamma)C_L - (v_a + w_x\cos\gamma - w_z\sin\gamma)C_D] \\ & - \mathbf{v}_a^T[\nabla\mathbf{w}]\mathbf{v} - 2\mathbf{v}_a^T[\nabla\mathbf{w}]\mathbf{w} - \mathbf{w}^T[\nabla\mathbf{w}]\mathbf{w}\end{aligned} \tag{25}$$

where $\mathbf{v}_a^T = [\,v_a\cos\gamma \quad -v_a\sin\gamma\,]$ (i.e., air speed expressed in the inertial frame).

The last three terms in Eq. (25) define the contribution of wind gradient to power. Remembering that z is positive down, we can see that negative gradients contribute to positive power (i.e., both increasing upward wind and increasing headwind allow power extraction from the gradient).

B. Trajectory Optimization

Given the vehicle dynamics, the energy-extraction problem can be cast as a trajectory optimization problem:

$$\text{minimize} \quad C(\mathbf{x}, \mathbf{u}) \tag{26}$$

$$\text{subject to } \dot{\mathbf{x}} = f(\mathbf{x}, \mathbf{u}, \mathbf{w}) \tag{27}$$

$$\mathbf{x}_{\min} \le \mathbf{x} \le \mathbf{x}_{\max} \tag{28}$$

$$\mathbf{u}_{\min} \le \mathbf{u} \le \mathbf{u}_{\max} \tag{29}$$

where C is a cost function (discussed subsequently), Eq. (27) defines constraints on vehicle dynamics, Eq. (28) defines constraints on the state (for example, minimum altitude or minimum/maximum air speed), and Eq. (29) defines constraints on control inputs (for example, control-surface deflections).

The choice of cost function is critical in the trajectory that is eventually computed and may vary depending on mission. For example, maximum endurance can be obtained by minimizing power, maximum range can be obtained by maximizing L/D, and minimum time can be obtained by maximizing velocity.

Here, we will maximize $\Delta E/\Delta x$, the change in total energy with respect to distance. Note that in gliding flight in still air, this quantity will always be negative, representing energy loss (a steady loss of altitude when air speed is constant). For gliding flight,

$$\begin{aligned}\frac{\Delta E}{\Delta x} = \frac{\dot E}{\dot x} = -\frac{1}{(v_a\cos\gamma + w_x)}\Bigg[& q\frac{S}{m}((w_x\sin\gamma + w_z\cos\gamma)C_L \\ & + (v_a + w_x\cos\gamma - w_z\sin\gamma)C_D) + \mathbf{v}_a^T[\nabla\mathbf{w}]\mathbf{v} + 2\mathbf{v}_a^T[\nabla\mathbf{w}]\mathbf{w} \\ & + \mathbf{w}^T[\nabla\mathbf{w}]\mathbf{w}\Bigg]\end{aligned} \tag{30}$$

This has units of acceleration.

If information about the future wind field is available (for example, if a pure sinusoidal gust field is assumed, as by Lissaman and Patel [6]), then a sequence of inputs to maximize average $\Delta E/\Delta x$ over a time interval can be computed. This time interval could be one period of the dominant frequency of the gust field or it could be some receding horizon. However, if this information is not available (or if it is too uncertain to be useful), then we must compute an input to maximize the instantaneous value of $\Delta E/\Delta x$, given knowledge only of current wind.

Simply computing C_L to maximize instantaneous $\Delta E/\Delta x$ will result in minimizing C_L (i.e., pushing the nose down to maximize air speed). To avoid this we compute the C_L that maximizes energy gain (or, equivalently, minimizes energy loss) while imposing steady glide constraints. In a steady glide,

$$L = mg\cos\gamma = qSC_L \tag{31}$$

$$D = -mg\sin\gamma = qSC_D \tag{32}$$

and hence $-\tan\gamma = C_D/C_L$. Further, assuming that γ is small,

$$C_L = \frac{mg}{qS} \tag{33}$$

and the instantaneous energy change for a particular value of $\mathbf{w}$ and $\nabla\mathbf{w}$ is now a function of only air speed. Note that in zero wind, Eq. (30) simplifies to

$$\frac{\dot{E}}{\dot{x}} = -\frac{1}{v_a \cos\gamma} q \frac{S}{m} v_a C_D = -g \frac{C_D}{C_L}$$

and so maximizing energy change in zero wind means minimizing C_D/C_L (i.e., flying at the best L/D).

The optimal (steady-state) air speed can be found using standard bounded function minimization tools such as MATLAB's `fminbnd`, and the angle of attack can be computed from the associated optimal lift coefficient. The state that maximizes energy change is denoted as $\mathbf{x}_{ss,\text{opt}}$ and it comprises $[\theta_{ss,\text{opt}}\ v_{a_{ss,\text{opt}}}\ \alpha_{ss,\text{opt}}\ 0]$. Note that the optimal pitch rate is zero in this steady-state approximation.

Clearly, the air speed and angle of attack computed using this approach is suboptimal, because it does not allow full exploitation of the aircraft dynamics. However, the steady-state approximation allows us to determine an air speed and angle of attack using only information available at the current instant; it does not require predictions of future wind, which are required by cyclic or receding-horizon approaches.

C. Speed to Fly

Given the steady-state approximation, the optimal speed to fly can be computed for a particular aircraft for various values of $\mathbf{w}$ and $\nabla\mathbf{w}$. In this example, we use an RnR Products SB-XC with parameters given in Table A1 in Appendix A. Results are given in Fig. 2.

Figure 2a shows the best speed to fly under the steady-state approximation. Two heavy black lines indicate the zero gradient case (i.e., constant vertical wind speed) and the zero vertical wind speed case. In zero gradient the aircraft flies slowly in rising air (negative values of w_z) and quickly in downward moving air; this behavior will result in the well-known strategy of dolphin soaring. It is interesting to note the effect of wind gradients on the best speed to fly: a significant jump occurs when the wind gradient is strongly upward, indicating that if the aircraft flies into a strong upward gradient, it should increase its speed, not decrease it (as in dolphin soaring). This behavior of flying fast through a strong gradient is also noted by Qi and Zhao [23]. The speed to fly is limited by the aircraft's maximum speed, hence the flat plateau on the surface plot.

Figure 2b shows the energy that can be extracted. There is a clear change in slope along the boundary at which the maximum speed is optimal, indicating that a significant amount of energy is available from the gradient of the vertical wind speed and not just from the vertical component of wind alone.

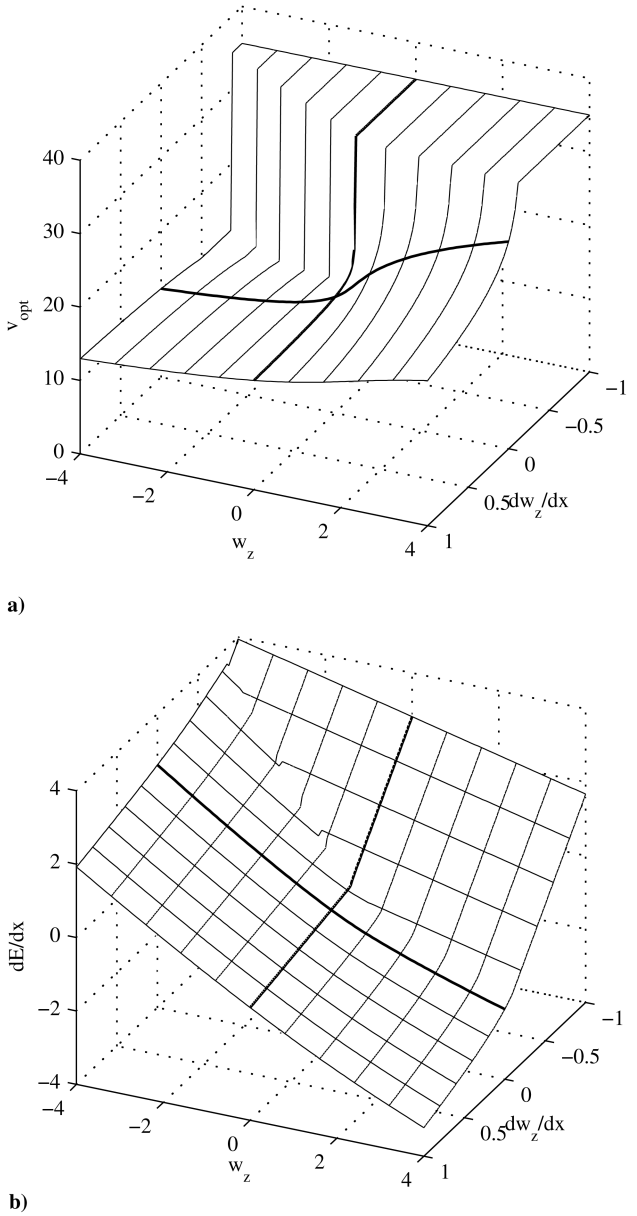

Fig. 2 Speed to fly and energy available depending on vertical wind speed and gradient.

IV. Control Architecture

Now that an optimal vehicle state has been computed (or, in the case of a receding-horizon control, a sequence of optimal states), a command-following controller must be designed and implemented. A standard approach is to design an inner-loop controller (for example, capable of following commanded states or desired outputs) with the outer loop comprising the receding-horizon control computation. This is shown schematically in Fig. 3.

In the research presented here, the assumption of steady glide precludes the necessity for predictive control, and only the current wind is needed for computing the optimal state. In effect, this is a receding-horizon controller with a one-step planning horizon.

The remainder of this paper is concerned with the inner-loop control problem. Actually following commanded states in gusty conditions using limited control inputs (e.g., only elevators) is a difficult problem, and the ability to follow the commanded states will have a large effect on actual energy extraction. The problem, therefore, is designing an inner-loop controller that maximizes energy extraction given the commanded sequence of optimal states while respecting limitations such as saturation.

Although the methodology presented here is general, as an example, a closed-loop controller is designed for an RnR Products SB-XC aircraft (parameters given in Table A1 of Appendix A). This aircraft is equipped with flaps, but only elevator control is considered here.

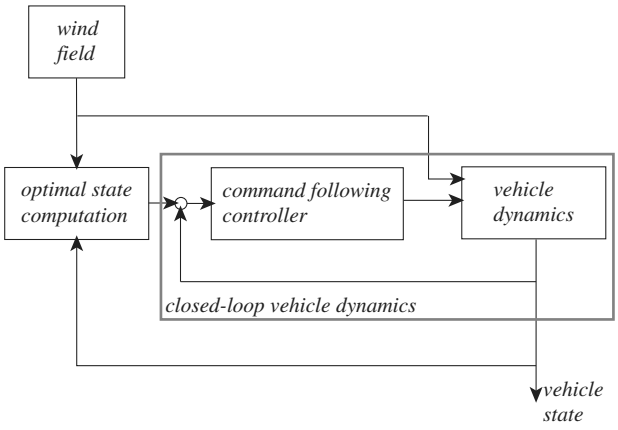

Fig. 3 Inner- and outer-loop control employing energy-maximization computation. This energy maximization may be a receding-horizon controller (if some a priori knowledge of wind field is available).

A. Inner-Loop Control Design

To simplify the problem of feedback control, system dynamics can linearized about some trim condition (here, steady flight at the best L/D air speed), and a state feedback controller can be designed for small perturbations about this trim condition:

$$\delta_e = -\mathbf{K}(\mathbf{x} - \mathbf{x}_{\text{trim}}) + \delta_{e,\text{trim}} \tag{34}$$

where δ_e is elevator deflection.

In the implementation considered here, the controller attempts to regulate the states to $\mathbf{x}_{ss,\text{opt}}$, and so

$$\delta_e = -\mathbf{K}(\mathbf{x} - \mathbf{x}_{ss,\text{opt}}) + \delta_{e,\text{trim}} \tag{35}$$

The gain matrix $\mathbf{K}$ can be determined using techniques such as pole placement or a linear quadratic regulator (LQR). This approach assumes that the change in linearized system dynamics is small over the range of states likely to be encountered during flight through the gust field, and so a particular choice of $\mathbf{K}$ is appropriate over a wide speed range. This approach also assumes that $\delta_{e,\text{trim}}$ does not change significantly. Both of these assumptions are likely to make the final solution brittle, but in the simulation results presented here, good results are still obtained. It may be possible to use techniques such as gain scheduling to improve performance.

Here, a controller was designed using a linear quadratic regulator, which seeks to minimize a cost function J_c:

$$J_c = \int ((\mathbf{x} - \mathbf{x}_{\text{des}})^T \mathbf{Q}(\mathbf{x} - \mathbf{x}_{\text{des}}) + \mathbf{u}^T \mathbf{R}\mathbf{u})\mathrm{d}t \tag{36}$$

where the state vector is $\mathbf{x}^T = [\theta\ v_a\ \alpha\ Q]^T$, $\mathbf{x}_{\text{des}}$ is the desired state vector, and the input is $\mathbf{u} = \delta_e$. The components of $\mathbf{Q}$ and $\mathbf{R}$ represent the relative importance of regulating states versus control cost.

The problem now is the choice of weight matrices $\mathbf{Q}$ and $\mathbf{R}$ that will maximize energy gain in the control architecture of Fig. 3. For example, a large value of Q_{33} and small value of Q_{11} implies that angle of attack must be controlled more precisely than the pitch angle.

Because $\mathbf{Q}$ and $\mathbf{R}$ define relative importance, we can set a particular component to 1 without loss of generality. To limit the dimension of the space of possible controllers, Q_{33} was set to 1 and Q_{44} was set to 1×10^{-9}. The small value of Q_{44} was chosen because the optimal value of pitch rate determined using the steady-state approximation is zero, and the true optimal value of pitch rate is likely to be significantly different for the dynamic case. The remaining free parameters Q_{11} and Q_{22} are the relative importance of pitch angle and air speed with respect to angle of attack, respectively, and R is the relative importance of control cost.

Here, we determine the optimal state cost and control cost to maximize energy change for flight through a sinusoidally varying vertical gust field. The gust field is assumed to be frozen in space; that is,

$$w_z(x_i) = \sqrt{2}\sigma_z \sin\frac{2\pi x_i}{L_w} \tag{37}$$

Three gust wavelengths are considered: 25, 50, and 100 m. For each case, the root-mean-square vertical velocity $\sigma_z = 2\ \text{m} \cdot \text{s}^{-1}$. Simulations of flight 1000 m in length through the each gust field using controllers computed using various values of Q_{11}, Q_{22}, and R were conducted to evaluate a reward function J:

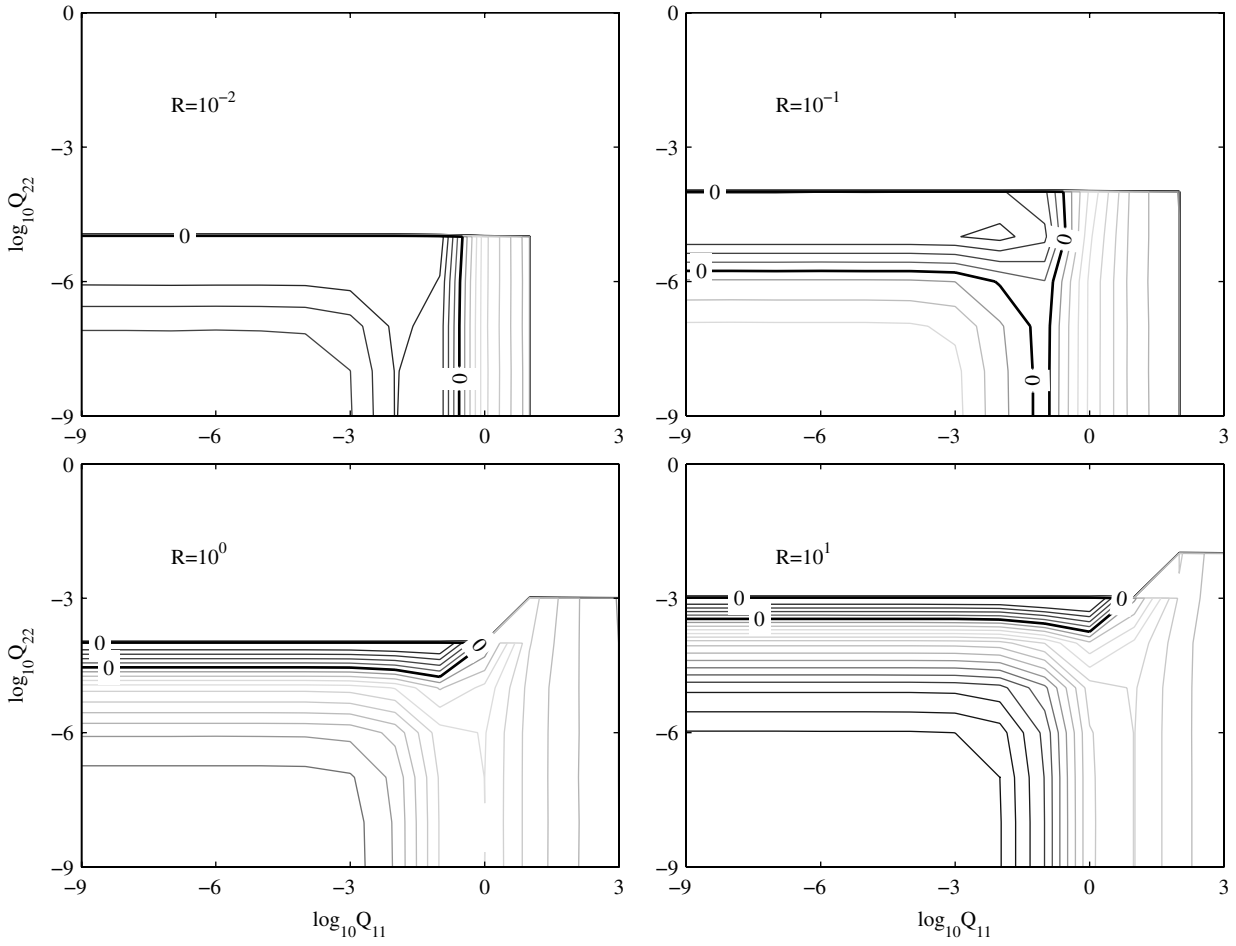

Fig. 4 Contours of change in energy vs weights for flight through a sinusoidal gust field with $\sigma_z = 2$ m/s and $L_w = 50$ m. The heavy black line shows the contour for $\Delta E_{\text{tot}} = 0$.

$$J = \begin{cases} \Delta E_{\text{tot}} & \text{if } \mathbf{x}_{\min} \leq \mathbf{x} \leq \mathrm{x}_{\max} \\ -9999 & \text{otherwise} \end{cases} \tag{38}$$

The state limits $\mathbf{x}_{\min}$ and $\mathbf{x}_{\max}$ ensure feasibility of the trajectory and are defined in Table A2 in Appendix A.

Figure 4 shows contour plots of ΔE_{tot} for one gust case: $L_w = 50$ m. The heavy black line shows the contour for $\Delta E_{\text{tot}} = 0$; regions inside this contour denote energy *gain* through the gust field. The region outside all contours denotes values of Q_{11} and Q_{22} for which state limits were exceeded and thus denotes the infeasible region of the weight space.

The control weight R varied from 10^{-3} to 10. As control gets "cheaper" (i.e., smaller values of R), the region of energy gain gets larger. It is interesting to note, however, that maximum energy gain does not occur at minimum R (note shown in Fig. 4): this occurs when $R = 10^{-2}$. Also, the range of values of Q_{11} for which energy gain is possible is significantly larger than the range of values of Q_{22}. In steady-state gliding, flight angle of attack and air speed are directly related. It should therefore come as no surprise that air speed is given some weight in the control design. However, tracking an air-speed command in gusty conditions using only an elevator is more difficult than tracking an angle-of-attack command, because the time constant of air speed with respect to the elevator is much slower than the time constant of angle of attack. Higher values of Q_{22} result in the aircraft chasing the desired air speed.

The maximum change in energy and optimal values of state and control weight are given in Table 1 for the three gust lengths. Energy gain is possible for all three gust lengths, but the 50 m gust allows significantly better energy extraction. Note also that the optimal weights differ for each of the gust lengths: a controller synthesized to maximize energy gain from a 25 m gust may perform poorly over the 100 m gust. One approach to handling multiple gust lengths is to set up a gain-scheduling controller, but this requires knowledge of the gust length. A simpler approach is to synthesize a controller based on the best value of mean energy extraction (taken over the three gust lengths). The last column of Table 1 shows the energy gain for each gust length using a controller synthesized from the optimal mean weights, and Fig. 5 shows energy contours averaged over the three gust lengths. The largest energy gain occurs when $R = 10^{-2}$; no energy is gained when $R \geq 1$.

Table 1 Optimal change in energy and LQR weights

L_w	Best ΔE	Q_{11}	Q_{22}	R	$\Delta E_{\text{mean}Q}$[b]
25	83.25	10^{-1}	10^{-9}	10^{-3}	17.67
50	201.43	10^{-2}	10^{-5}	10^{-2}	199.5
100	20	10^{-9}	10^{-6}	10^{-2}	-33.7
Mean[a]	61	10^{-5}	10^{-5}	10^{-2}	

[a]The bottom row shows the optimal mean change in energy over the 3 gust lengths.
[b]The rightmost column shows the change in total energy for each gust length using weights that maximize mean energy change.

Using $Q_{11} = 10^{-5}$, $Q_{22} = 10^{-5}$, and $R = 10^{-2}$, the final controller gains are

$$\mathbf{K} = [\,1.0106 \quad -0.0277 \quad 5.8082 \quad 0.5847\,] \tag{39}$$

The combination of the optimal steady-state energy-extraction computation of Sec. III.B with the state feedback controller defined previously (referred to as a "gust-soaring controller") enables energy extraction from flight through gusts.

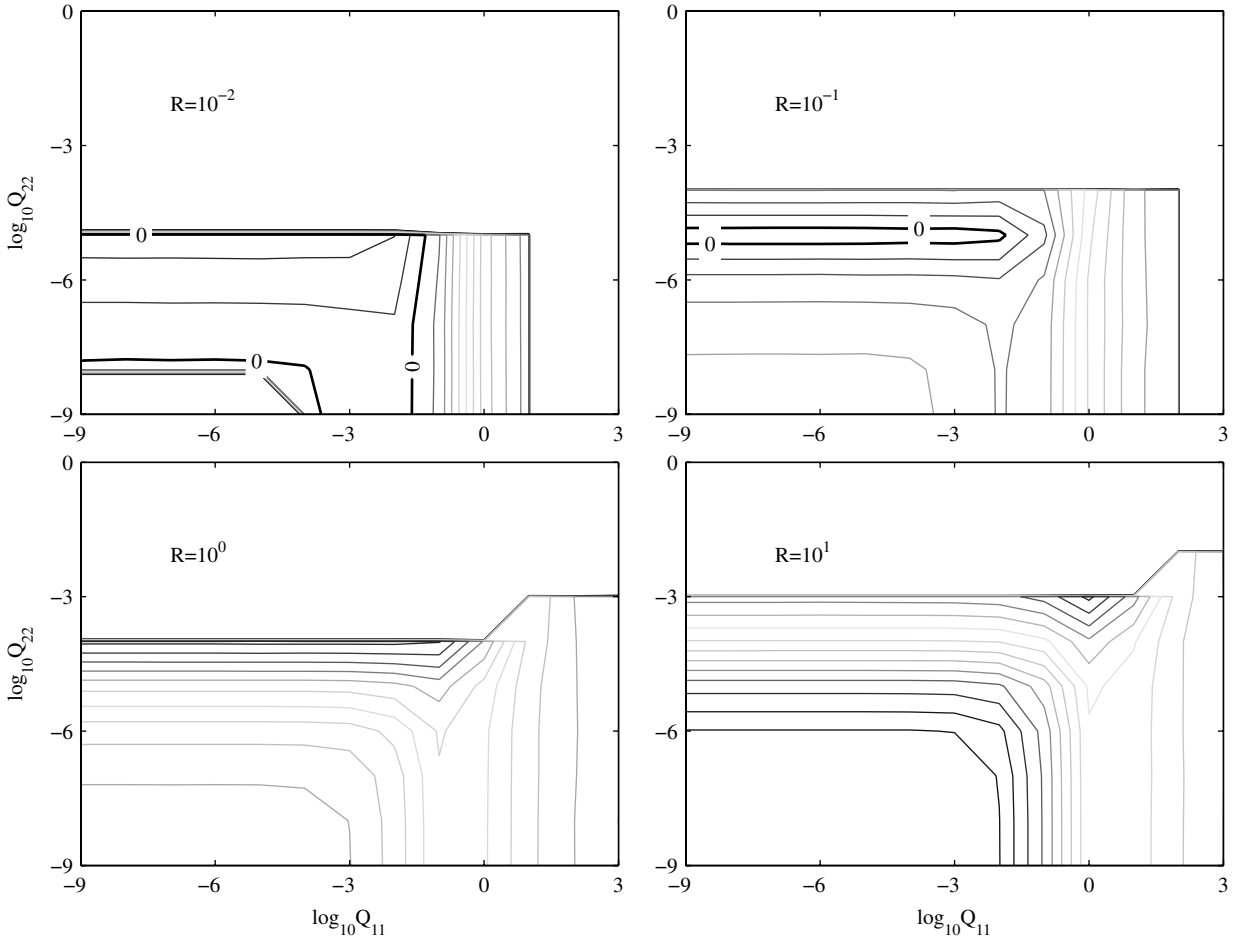

Fig. 5 Contours of mean change in energy vs weights for flight through sinusoidal gust fields with $\sigma_z = 2$ m/s, averaged over $L_w = 25$, 50, and 100 m. The heavy black line shows the contour for $\Delta E_{\text{tot}} = 0$.

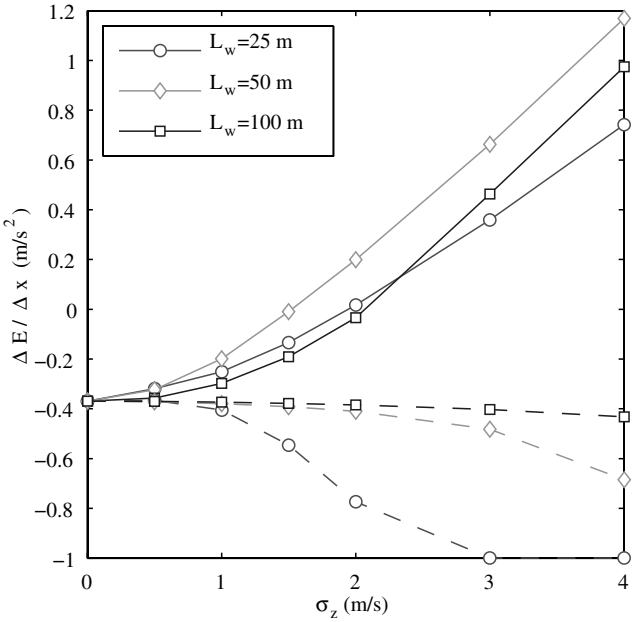

Fig. 6 Energy change for 1000 m flight through various sinusoidal gust fields. The solid lines show results for the gust-soaring controller, dashed lines show results using a constant-air-speed controller. Cases for which state limits are exceeded are shown by fixing the energy change to −1.

V. Simulation and Discussion

Simulations of flights using the gust-soaring controller were conducted for sinusoidally varying gust fields and for flights through fields of randomly distributed thermals. For comparison, results are also presented for simulated flights using a constant-air-speed controller (to maintain flight at the best L/D in calm air) synthesized using output regulation (using MATLAB's `lqry` command). As with the gust-soaring controller, vehicle dynamics were linearized about trimmed flight at the best L/D.

A. Sinusoidal Gust Fields

To assess the effectiveness of the gust-soaring controller over various gust fields and to assess the range of gust conditions over which energy extraction is possible, a sequence of simulations of flight through sinusoidal gust fields of varying wavelength and root-mean-square vertical wind velocity was conducted. In all cases, simulations of flights of 1000 m were conducted. Results are given in Fig. 6, which shows the energy change for the gust-soaring controller as well as for the air-speed-regulating controller.

Using the gust-soaring controller, net energy gain is possible for each of the gust fields considered. For the 50 m wavelength, gust-field net energy gain occurs when $\sigma_z > 1.55\ \mathrm{m \cdot s^{-1}}$. Results presented by Lissaman and Patel [6] indicate that energy neutral trajectories for a vehicle with the best $L/D \approx 25$ at this wavelength are achievable with a root-mean-square gust intensity of approximately $1.13\ \mathrm{m \cdot s^{-1}}$. However, this assumes 1) full knowledge of future wind speeds so that the optimal trajectory can be computed and 2) that the optimal trajectory so computed can be flown exactly. Here, a suboptimal state is computed without knowledge of future wind speeds, and elevator control is used to regulate the vehicle state to the desired values.

As a comparison, an output-regulating controller was synthesized using MATLAB's `lqry` command with air speed as the output and elevator deflection as the input. As for the gust-soaring controller, system equations were linearized about the best L/D speed for this vehicle. Reduced performance (i.e., energy loss greater than that observed for steady flight in still air) is shown for the case of constant-air-speed flight through each of the gust fields. For the 25 m gust field, state limits are exceeded for rms wind speeds greater than $3\ \mathrm{m \cdot s^{-1}}$.

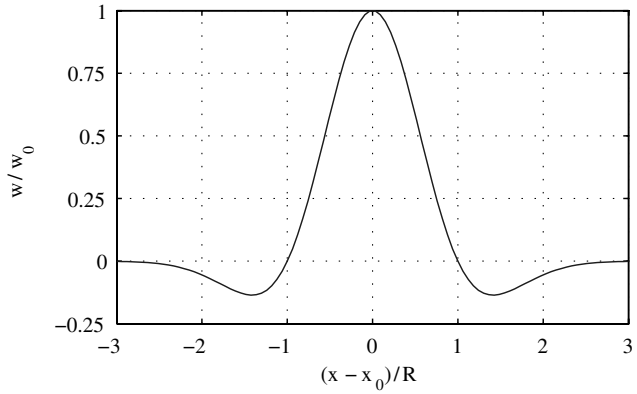

Fig. 7 Normalized vertical wind profile for the Gedeon thermal model.

B. Thermal Fields

Because it is not clear that they are appropriate for small and micro UAVS, rather than test the controller on a Dryden or von Kármán gust field, we will simulate flight of the vehicle through a field of randomly placed thermals.

For a single thermal, the vertical wind velocity is computed using a model presented by Gedeon [14] and used in several studies of optimal flight trajectories [23]:

$$w_z(x) = w_0 e^{-\left(\frac{x-x_0}{R}\right)^2}\left[1 - \left(\frac{x-x_0}{R}\right)^2\right] \tag{40}$$

where w_0 is the maximum vertical wind speed, x_0 is the thermal center, and R is the thermal radius. This model provides a region of sinking air immediately around the rising central core, which has been observed by glider pilots. The *area of effect* of a thermal is approximately 3 times the thermal radius. This thermal profile is shown in Fig. 7.

For a sequence of N thermals, the total vertical wind speed is

$$w_z(x) = \sum_{n=1}^{N} w_{0,n} e^{-\left(\frac{x-x_n}{R_n}\right)^2}\left[1 - \left(\frac{x-x_n}{R_n}\right)^2\right] \tag{41}$$

A field of 150 thermals was randomly generated using uniform distributions over the ranges of variables given in Table 2. The vehicle was flown for 5000 m through this thermal field using both the gust-soaring controller and the air-speed-regulating controller. Results of a Monte Carlo simulation of flights through 50 random

Table 2 Parameters for thermal field

Variable	Range	Description
w_0	5 to −5	Maximum vertical wind speed (positive down)
R	10 to 20	Thermal radius

Table 3 Summary of thermal-field results

	Minimum $\Delta E/\Delta x$	Mean $\Delta E/\Delta x$	Maximum $\Delta E/\Delta x$
gust-soaring	−0.34	−0.27	−0.19
Constant speed	−0.46	−0.37	−0.28
% improvement	26%	27%	32%

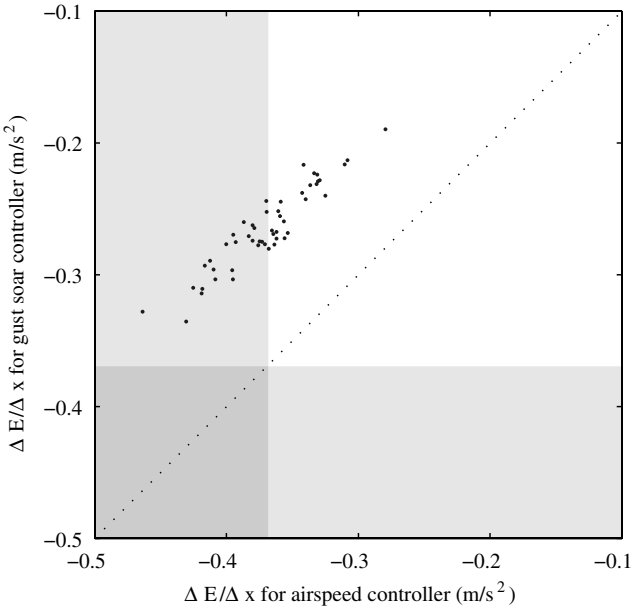

Fig. 8 Energy change using gust-soaring controller vs constant-air-speed controller.

thermal fields are shown in Fig. 8. The average value of the root-mean-square vertical wind speed over the 50 runs was 1.1 m/s.

For all runs, the gust-soaring controller significantly outperformed constant-air-speed flight (all points are above the dotted line that denotes equal performance). For this aircraft, the energy change for steady glide in still air is approximately -0.37 m $\cdot$ s^{-2}. All points that lie to the left of -0.37 (shown by the vertical shaded region) show cases in which the air-speed-regulating controller resulted in worse performance than would have been obtained in calm air; no points lie below -0.37, and hence the gust-soaring controller was always able to extract energy from the wind field. Results are tabulated in Table 3. The mean energy change with the gust-soaring controller is -0.27 m $\cdot$ s^{-2}, which agrees very well with the mean energy change observed with flight through a sinusoidal gust field with a rms vertical wind speed of 1.1 m/s (Fig. 6). The gust-soaring controller results in energy savings of up to 32% compared with the air-speed-regulating controller.

Results for a single representative run are presented in Fig. 9. The plot of total energy shows that the gust-soaring controller immediately shows better performance than the constant-air-speed controller.

It should not be surprising that more control effort (evidenced by the greater elevator deflection) is required by the gust-soaring controller than by the constant-air-speed control. However, significant control effort is still required for the air-speed-regulating controller, and there is a large benefit to employing gust-soaring control. Further, careful design of control surfaces and selection of appropriate actuators should reduce the energy required for control-surface actuation. Thus, even when the energy required for control actuation is taken into consideration, it is likely that significant energy savings will result from gust soaring.

VI. Conclusions

This paper has presented a closed-loop architecture for gust energy extraction for small and micro uninhabited aerial vehicles. The architecture consists of an optimal state computation (for example, a receding-horizon controller) combined with a command-following controller. The contributions of this paper are 1) computation of the state that maximizes energy gain and 2) design of the command-following controller using state feedback. Results of simulations show the energy gain that is possible with this approach.

The optimal state computation is performed by maximizing the energy change over distance for flight through a spatially varying wind field. The energy change is computed using a full model of aircraft longitudinal dynamics. To enable closed-loop control, the

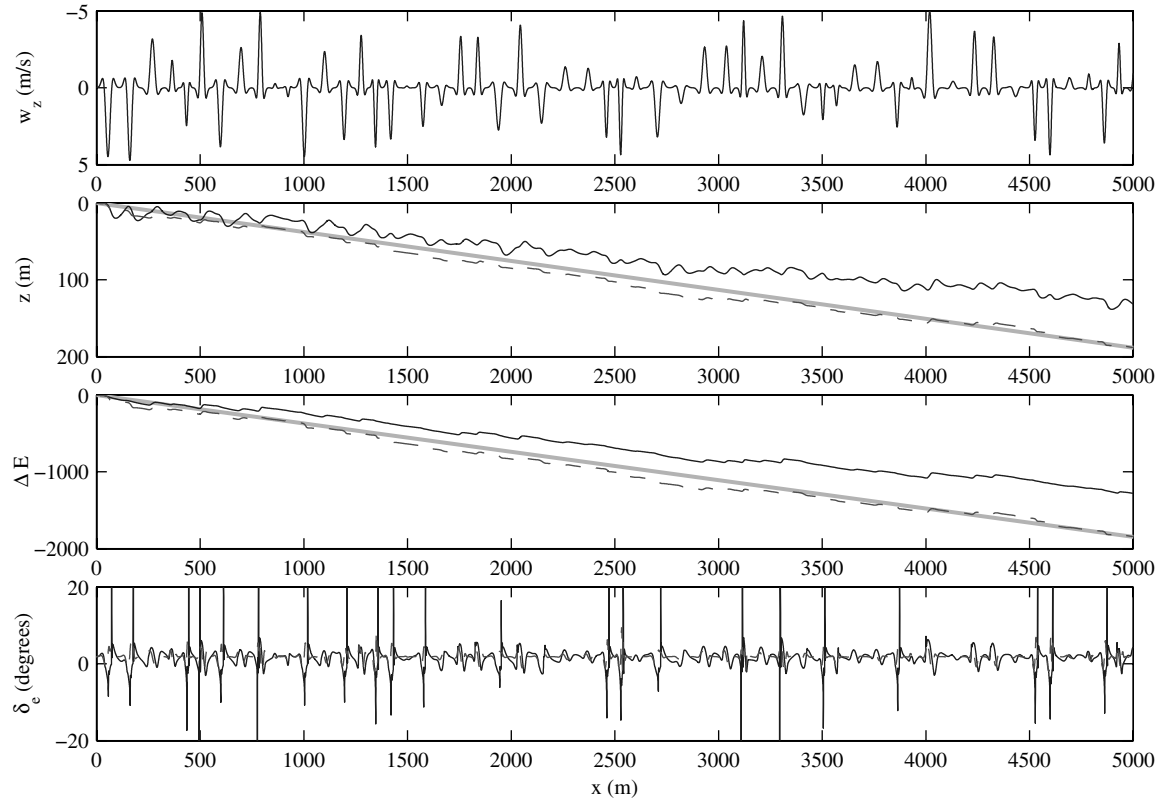

Fig. 9 Flight through a field of random thermals. The solid line shows results using the gust-soaring controller. The dashed line shows results from the constant-air-speed controller. The upper plot shows the vertical wind speed, the second plot shows the flight path, the third plot shows change in total energy, and the fourth plot shows elevator deflection. The wide gray line shows the flight path and energy change for steady flight in calm air.

Table A1 Parameters for SB-XC glider

Variable	Value	Description
m	10 kg	Mass
b	4.34 m	Span
c	0.232 m	Mean aerodynamic chord
S	1 m^2	Wing area
I_{yy}	1.87 $kg \cdot m^2$	Pitch moment of inertia
C_{L0}	0.37	——
C_{L_α}	5.54/rad	——
C_{L_Q}	−3.255 s/rad	——
$C_{L_{\dot{\alpha}}}$	−0.651 s/rad	——
$C_{L_{\delta_e}}$	−0.37/rad	——
$C_{L_{\delta_f}}$	1.63/rad	——
$f_{LD}(\varphi)$	$0.1723\varphi^4 - 0.3161\varphi^3 + 0.2397\varphi^2 - 0.0624\varphi + 0.0194$	$\varphi = C_{L0} + C_{L_\alpha}\alpha$
$C_{D_{\delta_e}}$	0/rad	——
$C_{D_{\delta_f}}$	0.042/rad	——
C_{m0}	0	——
C_{m_α}	−1.02/rad	——
C_{m_Q}	−14.6 s/rad	——
$C_{m_{\delta_e}}$	1.6275/rad	——
$C_{m_{\delta_f}}$	−0.254/rad	——

Table A2 State limits and control saturation for the SB-XC glider

State/control	Range	Description
θ	−45–45 deg	Pitch
v_a	11–35 m/s	Air speed
α	−2–12 deg	Angle of attack
Q	−999–999	Pitch rate
δ_e	−20–20 deg	Elevator deflection

state that maximizes instantaneous energy gain using only current measurements of wind speed and gradient is computed; a prediction of the future wind field is not required.

To avoid unreasonable control inputs, the computation of instantaneous energy gain approximates the flight path with an assumption of steady gliding flight. Compared with approaches that assume knowledge of the future wind field, the sequence of states computed using this approach will necessarily result in suboptimal energy gain. However, it significantly reduces computational burden in addition to obviating the need for full a priori knowledge of the gust field.

A state feedback controller is used to follow the desired state. The controller is designed using LQR synthesis, and the critical problem is selection of the weighting matrices. Here, a search technique is used to determine the values of state and control cost weights that maximize energy gain for flight through sinusoidal gust fields of varying wavelength. As an example a gust-soaring controller was designed for a small autonomous glider with only elevator input.

Simulations of flights through sinusoidal gust fields of varying wavelength and root-mean-square vertical wind velocity show the effectiveness of this gust-soaring controller, and simulation of flight through thermal fields shows that significant improvement in flight performance is possible. Future work will include improvements to the energy-maximization computation.

Appendix A: Vehicle Properties

Simulation results are based on the RnR products SB-XC radio-control glider. Parameters in Table A1 were obtained from a drag-buildup computation; state limits in Table A2 were defined to limit states to reasonable bounds.

Note that a fourth-order polynomial is used to relate C_D to C_L: this provided a better fit to the computed data over the full speed range.

Acknowledgments

The author thanks Mark Maughmer for many insightful discussions and Götz Bramesfeld for the drag buildup and stability derivative computations for the SB-XC.

References

[1] Boslough, M. B. E., "Autonomous Dynamic Soaring Platform for Distributed Mobile Sensor Arrays," Sandia National Labs., TR SAND2002-1896, Albuquerque, NM, 2002.

[2] Kiceniuk, T., "Calculations on Soaring in Sink," *Technical Soaring*, Vol. 25, No. 4, Oct. 2001, pp. 228–230.

[3] Allen, M. J., and Lin, V., "Guidance and Control of an Autonomous Soaring Vehicle with Flight Test Results," AIAA Aerospace Sciences Meeting and Exhibit, AIAA Paper 2007-867, Reno, NV, Jan. 2007.

[4] Phillips, W. H., "Propulsive Eects due to Flight Through Turbulence," *Journal of Aircraft*, Vol. 12, No. 7, July 1975, pp. 624–626. doi:10.2514/3.44480

[5] Patel, C. K., and Kroo, I., "Control Law Design for Improving UAV Performance Using Wind Turbulence," AIAA Aerospace Sciences Meeting and Exhibit, AIAA Paper 2006-0231, Reno, NV, Jan. 2006.

[6] Lissaman, P. B. S., and Patel, C. K., "Neutral Energy Cycles for a Vehicle in Sinusoidal and Turbulent Vertical Gusts," 45th AIAA Aerospace Sciences Meeting and Exhibit, AIAA Paper 2007-863, Reno, NV, Jan. 2007.

[7] MacCready, P. B., Jr., "Optimum Air Speed Selector," *Soaring*, Jan.–Feb. 1958, pp. 10–11.

[8] Arho, R., "Distance Estimation Error and Stationary Optimal Gliding," *OSTIV Publication XII*, Organisation Scientifique et Technique Internationale du Vol a Voile, Delft, The Netherlands, 1972.

[9] Metzger, D. E., and Hedrick, J. K., "Optimal Flight Paths for Soaring Flight," *Journal of Aircraft*, Vol. 12, No. 11, 1975, pp. 867–871. doi:10.2514/3.59886

[10] de Jong, J. L., "The Convex Combination Approach: A Geometric Approach to the Optimization of Sailplane Trajectories," *OSTIV Publication XVI*, Organisation Scientifique et Technique Internationale du Vol a Voile, Delft, The Netherlands, 1981, pp. 182–201.

[11] Cochrane, J. H., "MacCready Theory with Uncertain Lift and Limited Altitude," *Technical Soaring*, Vol. 23, No. 3, July 1999, pp. 88–96.

[12] Irving, F., "The Energy Loss in Pitching Manoeuvres," *Proceedings of the XVI OSTIV Congress*, Organisation Scientifique et Technique Internationale du Vol a Voile, Delft, The Netherlands, 1978.

[13] Gedeon, J., "The Inuence of Sailplane Performance and Thermal Strength on Optimal Dolphin-Flight Transition Piloting Techniques," *Proceedings of the XV OSTIV Congress*, Organisation Scientifique et Technique Internationale du Vol a Voile, Delft, The Netherlands, 1976.

[14] Gedeon, J., "Dynamic Analysis of Dolphin Style Thermal Cross Country Flight," *Proceedings of the XIV OSTIV Congress*, Organisation Scientifique et Technique Internationale du Vol a Voile, Delft, The Netherlands, 1974.

[15] Zhao, Y. J., "Optimal Patterns of Glider Dynamic Soaring," *Optimal*

Control Applications and Methods, Vol. 25, No. 2, 2004, pp. 67–89. doi:10.1002/oca.739

[16] Zhao, Y. J., and Qi, Y. C., "Minimum Fuel Powered Dynamic Soaring of Unmanned Aerial Vehicles Utilizing Wind Gradients," *Optimal Control Applications and Methods*, Vol. 25, No. 5, 2004, pp. 211–233. doi:10.1002/oca.744

[17] Sachs, G., and Mayrhofer, M., "Shear Wind Strength Required for Dynamic Soaring at Ridges," *Technical Soaring*, Vol. 25, No. 4, Oct. 2001, pp. 209–215.

[18] Sachs, G., "Minimum Shear Wind Strength Required for Dynamic Soaring of Albatrosses," *Ibis*, Vol. 147, 2005, pp. 1–10. doi:10.1111/j.1474-919x.2004.00295.x

[19] Pennycuick, C. J., "Gust Soaring as a Basis for the Flight of Petrels and Albatrosses (Procellariformes)," *Avian Science*, Vol. 2, No. 1, 2002, pp. 1–12.

[20] Lissaman, P., "Wind Energy Extraction by Birds and Flight Vehicles," 43rd AIAA Aerospace Sciences Meeting and Exhibit, AIAA Paper 2005-241, Reno, NV, Jan. 2005.

[21] Pierson, B. L., and Chen, I., "Minimum Altitude Loss Soaring in a Specied Vertical Wind Distribution," *Science and Technology of Low Speed and Motorless Flight*, CP 2085, edited by P. W. Hanson, NASA, Hampton, VA, Mar. 1979, pp. 305–318.

[22] *Aerosim: Aeronautical Simulation Blockset Users Guide*, Ver. 1.2, Unmanned Dynamics, Hood River, OR, 2004; also http://www.u-dynamics.com/aerosim/default.htm [retrieved Aug. 2008].

[23] Qi, Y. C., and Zhao, Y. J., "Energy-Efficient Trajectories of Unmanned Aerial Vehicles Flying Through Thermals," *Journal of Aerospace Engineering*, Vol. 18, No. 2, Apr. 2005, pp. 84–92. doi:10.1061/(ASCE)0893-1321(2005)18:2(84)